ChemComm

Accepted Manuscript

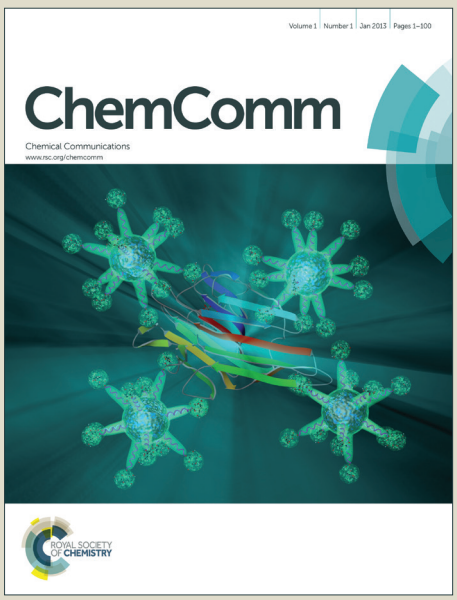

ROYAL SOCIETY OF CHEMISTRY

www.rsc.org/chemcomm

Cite this: DOI: 10.1039/c0xx00000x

www.rsc.org/xxxxxx

ARTICLE TYPE

Ultra-small gold nanoparticles immobilized on mesoporous silica/graphene oxide as highly active and stable heterogeneous catalysts

Li Peng, Jianling Zhang*, Shuliang Yang, Buxing Han, Xinxin Sang, Chengcheng Liu, Xue Ma and Guanying Yang

Received (in XXX, XXX) Xth XXXXXXXXX 20XX, Accepted Xth XXXXXXXXX 20XX
DOI: 10.1039/b000000x

Here we demonstrate the in situ formation of ultra-small gold nanoparticles (<2 nm) finely dispersed on a binary solid carrier, i.e. the mesoporous SiO_2 coated graphene oxide (GO) nanosheet. The as-synthesized Au/SiO_2/GO composite has shown highly catalytic activity and reusability for chemical reactions under mild conditions.

Metal nanoparticles of small size are the choice for catalyzing many reactions such as oxidation of alcohols and aldehydes, epoxidation, hydrochlorination, due to the increased specific surface areas and high density of edges and corner atoms.[1-3] However, small metal nanoparticles aggregate easily and usually form large particles, which reduces their catalytic activities.[4] To impede nanoparticle aggregation, the solid support (e.g. metal oxide, carbonaceous material, polymer, porous silica, etc) is usually required.[5-7] Among the diverse kinds of supports, graphene oxide (GO) has recently arisen as a promising support of metal nanoparticles,[8-12] because of its unique features such as high surface/weight ratio, accessible surface and controllable chemical composition.[13,14] Nevertheless, all the GO-supported gold nanoparticles reported are subject to limitation of large particle size from 5 nm to hundreds nanometers. In general, the gold nanoparticles that can activate the reactant molecules under mild conditions are generally <5 nm in diameter.[2]

Here we report the formation of ultra-small gold nanoparticles on a binary solid carrier, i.e. the mesoporous SiO_2 coated GO nanosheet. The mesoporous SiO_2 can not only provide confinement for gold nanoparticles, thus restricting their further growth or aggregation, but also prevent the aggregation or restacking of GO nanosheets. Moreover, from the view point of catalysis, the mesostructure of SiO_2 layer can facilitate the diffusion of substrates and products because of large surface area, and thus accelerate the reaction rate.[15] The Au/SiO_2/GO composite combines the advantages of small gold nanoparticles, mesoporous silica and GO nanosheet.

A one-pot strategy was designed for forming the Au/SiO_2/GO composite. The desired amounts of tetraethyl orthosilicate (TEOS) and $HAuCl_4$ were dissolved in TX-100 aqueous solution dispersed with GO, followed by the addition of compressed CO_2. The aim of utilizing compressed CO_2 is that it can react with water to form carbonic acid, which works as catalyst for TEOS hydrolysis; more importantly, compressed CO_2 can promote the deposition of nanoparticles on solid support.[16,17] The mixture was stirred at room temperature for 7 hours. Then CO_2 was released and the product was obtained after washing and drying.

Fig. 1 shows the TEM images of GO and the Au/SiO_2/GO composite synthesized at CO_2 pressure of 5.03 MPa. In contrast to the smooth surface of pure GO sheet (Fig. 1a), the surface of the Au/SiO_2/GO composite is rough by coating with a layer of porous silica (Figs. 1b and 1c). SEM image reveals that both sides of GO sheet are coated by a silica layer in thickness of ~10 nm (Fig. S1, ESI†). The nanoparticles are immobilized uniformly on the support, with a narrow size distribution 1.4-2.0 nm (Figs. 1d and 1e). The high-resolution TEM image shows the interplanar spacings for the lattice fringe of 0.208 nm (Fig. 1f), corresponding to (200) lattice plane of fcc metallic gold.

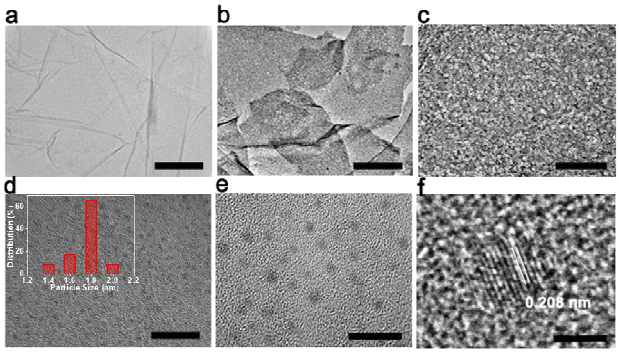

Fig. 1 TEM images of pure GO sheet (a) and Au/SiO_2/GO composite with different magnifications (b-f). Scale bars, 250 nm, 500 nm, 100 nm, 20 nm, 10 nm, and 2 nm for a, b, c, d, e, and f, respectively. The inset in d shows the particle size distribution.

The XRD pattern of the Au/SiO_2/GO composite is shown as curve a in Fig. 2. The peak at 2θ of 38° corresponds to 111 diffraction of fcc metallic gold (JCPDS PDF-04-0784). The other diffractions for gold crystal are hardly detected, resulting from the small size of gold nanoparticles.[18] The pure GO has a typical sharp peak at 9° corresponding to $d_{(002)}$ (curve c in Fig. 2).[19] However, this sharp peak disappears in the XRD pattern of Au/SiO_2/GO composite. It can be attributed to the formation of silica layer on GO surface, which prevents the restacking of GO.[19] The gold content in the Au/SiO_2/GO composite was determined to be 1.02 wt% by ICP-AES analysis.

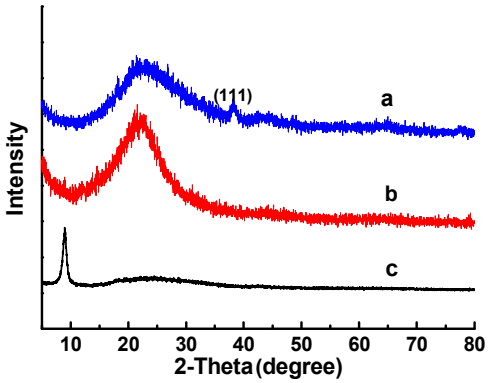

Fig. 2 XRD patterns of Au/SiO_2/GO composite (a), SiO_2 (b), and GO (c).

The porosity properties of the Au/SiO_2/GO composite were determined by N_2 adsorption-desorption method. A typical type-IV mode with a distinct hysteresis loop was observed for N_2 adsorption-desorption isotherms, proving that the silica layer is mesoporous (Fig. 3). The BET surface area and total pore volume are 429 m^2/g and 1.01 cm^3/g, respectively. The mesopore size distribution curve, calculated from Barrett-Joyner-Halenda method, shows a pore size distribution centered at 5.3 nm (the inset in Fig. 3).

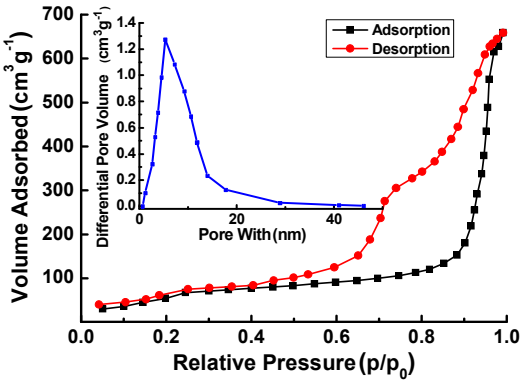

Fig. 3 N_2 adsorption-desorption isotherms and mesopore size distribution curve (the inset) of Au/SiO_2/GO composite.

The intermolecular interactions of the Au/SiO_2/GO composite were investigated by extended X-ray absorption fine structure (EXAFS) and X-ray photoelectron spectroscopy (XPS). The EXAFS spectra of the as-synthesized Au/SiO_2/GO composite and Au foil are shown in Fig. S2. By mathematical analysis and Fourier transform (see details in the electronic supplementary information), the Fourier transformed EXAFS spectra were obtained (Fig. 4a). Clearly, the Fourier transformed EXAFS of the Au/SiO_2/GO composite exhibits nearly identical features of the Au foil, indicating that the local environment of gold is unaffected by the presence of SiO_2/GO support.[20] For Au 4f XPS spectrum (Fig. 4b), the diffused peaks with binding energies of 84.2 and 88.0 eV coincide well with Au $4f_{5/2}$ and Au $4f_{7/2}$ in metallic state, respectively. It gives further support that the gold nanoparticles have no strong interactions with the support. The curve-fitting of Si 2p spectrum (Fig. 4c) shows a peak corresponding to Si−O−C bond at 102.8 eV, suggesting the covalent bonding between GO and silica.[19] Both EXAFS and XPS results prove the absence of strong interactions between gold nanoparticles and SiO_2/GO support. The formation of ultra-small nanoparticles results mainly from the confinement provided by the mesopores of silica layer.

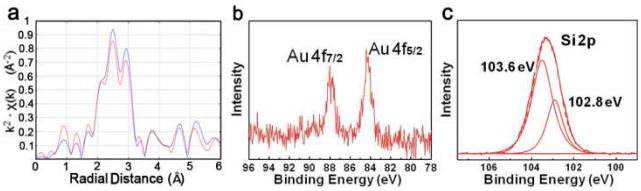

Fig. 4 a: Fourier transformed EXAFS functions of the Au/SiO_2/GO composite (red) and Au foil (blue) in the *R* domain. b, c: Au 4f and Si 2p XPS spectra of Au/SiO_2/GO composite, respectively.

The above results demonstrate the formation of ultra-small gold nanoparticles (<2 nm) dispersed uniformly in mesoporous SiO_2/GO. Such a structure makes them promising candidate of catalyst because the ultra-small gold nanoparticles can provide a high absolute number of active sites exposed[21] and the mesoporosity properties of the support can promote the diffusion of substrates and products.[15] Here the catalytic activities of the Au/SiO_2/GO composite for chemical reactions were detected. 4-Aminophenol (4-AP) is very useful and important in practical applications,[22,23] which is usually produced from the reduction of 4-nitrophenol (4-NP) in aqueous medium.[24] The light yellow aqueous 4-NP solution shows an absorption at ~317 nm, which shifts to 400 nm after the addition of sodium borohydride, corresponding to the formation of 4-nitorphenolate (Fig. 5a). Without catalyst, the UV spectrum is unchanged even after the reaction system is kept standing for 12 hours, indicating 4-AP cannot be formed. With the addition of a small amount of Au/SiO_2/GO composite (Au: 7.5 μmol/L), the absorption at 400 nm significantly decreases as the reaction proceeds (Fig. 5b). Meanwhile, a new absorption appears at 295 nm and gradually increases. It reveals the formation of 4-AP,[24] which was further confirmed by high performance liquid chromatography (Fig. S3). Within 3 minutes, 4-NP is reduced to 4-AP completely. The Au/SiO_2/GO catalyst is much more active than the Fe_3O_4@SiO_2-Au@mSiO_2 catalyst reported under the same experimental conditions, which needs 18 minutes for the complete reduction of 4-NP by using twenty times dosage of the Au/SiO_2/GO catalyst.[24] The recovered catalyst after running 14 cycles exhibits similar catalytic performance (Fig. S4, ESI†). The XRD patterns of the fresh catalyst and that after reused for 14 runs are almost the same (Fig. 5c), indicating that the structural integrity of the catalyst is well preserved. The TEM image of the catalyst after reused for 14 runs shows that the Au nanoparticles are free of any aggregation (inset of Fig. 5c). The high stability of the gold nanoparticles may result from the confinement of the mesoporous silica/GO support.

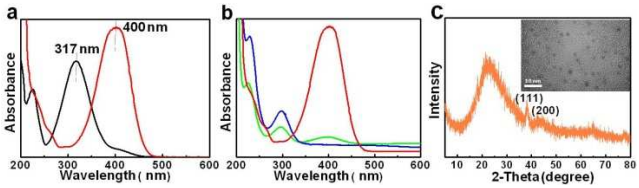

Fig. 5 Catalytic reduction of 4-nitrophenol catalyzed by $Au/SiO_2/GO$ composite. a: UV-vis spectra of 4-NP before (black) and after adding $NaBH_4$ solution (red). b: UV-vis spectra of the reduction process of 4-NP in aqueous solution using $Au/SiO_2/GO$ catalyst, reaction time: 1 min (green), 3 min (blue). c: XRD pattern and TEM image of the catalyst for the same reaction time (3 min) after running 14 cycles.

The styrene epoxidation is conventionally used to produce styrene oxide, which is an industrially important organic intermediate widely used in the synthesis of fine chemicals and pharmaceuticals.[25,26] The catalytic activities of the $Au/SiO_2/GO$ composite for styrene epoxidation were tested. As shown in Table 1, the styrene conversion increases monotonously with the reaction time, while the selectivity to styrene oxide first increases and then decreases after passing through a maximum value of 93.5% at 5 hours (Entries 1-5). The styrene could convert completely in 12 hours with 80.7% selectivity to styrene oxide (Entry 5). The turnover frequencies (TOF), defined as mole of substrate consumed per mole of gold per hour, could reach values higher than 400 h^{-1}. As far as we know, the catalytic activity of the $Au/SiO_2/GO$ catalyst is the highest among the reported Au catalysts ($Au/Fe_3O_4/SiO_2$,[24] Au/CaO,[25] Au/Yb_2O_3,[26] Au/Al_2O_3,[27] Au/HAP[28]) for styrene epoxidation by t-butyl hydroperoxide, of which the TOFs are in the range of 0.4-266 h^{-1}. The $Au/SiO_2/GO$ catalyst shows no evident drop of catalytic activity for the styrenne epoxidation after five runs (Entries 6-9). The TEM image of the catalyst after used five runs shows no particle aggregation (Fig. S5, ESI†) and no major difference was observed for the XRD patterns of the fresh and recovered catalysts (Fig. S6, ESI†).

Table 1 Styrene epoxidation catalyzed by $Au/SiO_2/GO$, Au/GO and Au/SiO_2.

Entry	Catalyst	Time /h	Conversion /%	Selectivity /%	TOF /h^{-1}
1	$Au/SiO_2/GO$	2	21.1	69.4	528
2	$Au/SiO_2/GO$	5	56.2	93.5	562
3	$Au/SiO_2/GO$	8	79.7	85.7	498
4	$Au/SiO_2/GO$	11	84.1	82.7	428
5	$Au/SiO_2/GO$	12	>99	80.7	417
6[a]	$Au/SiO_2/GO$	12	>99	82.0	417
7[b]	$Au/SiO_2/GO$	12	>99	82.0	417
8[c]	$Au/SiO_2/GO$	12	>99	82.0	417
9[d]	$Au/SiO_2/GO$	12	97	80.3	404
10	Au/GO	5	29.1	13.8	291
11	Au/GO	24	50.2	15.7	105
12	Au/SiO_2	5	7.5	50.1	75
13	Au/SiO_2	24	34.6	79.9	72
14	Au/Al_2O_3	5	16.3	28.1	152
15	Au/Al_2O_3	24	36	44.6	111

[a-d] $Au/SiO_2/GO$ catalyst for the second, third, fourth and fifth runs. Reaction conditions: Au (0.02 mol%), styrene (1.2 mL, 10 mmol), acetonitrile (15 mL), 5.0 g (38 mmol) of t-butyl hydroperoxide (70 wt% in water), N_2 balloon under atmospheric pressure, 80 °C.

For comparison, the binary Au/GO and Au/SiO_2 composites were synthesized by the method similar to that for the $Au/SiO_2/GO$ formation, in absence of TEOS and GO respectively. The Au/GO and Au/SiO_2 are much less active than the ternary $Au/SiO_2/GO$ catalyst for the above two reactions under the same experimental conditions (Fig. S7 and S8, ESI†, Entries 10-13 in Table 1). The TEM images show that the Au particles supported on SiO_2 suffer serious aggregation (Fig. S9, ESI†). It can be due to the fact that the mesopores of silica are too large (5-30 nm, Fig. S10 in ESI†) to provide confinement for gold nanoparticles. The Au particles supported on GO sheet are as large as 50-140 nm (Fig. S11, ESI†), resulting from the absence of a mesoposours structure (see N_2 adsorption-desorption results in Fig. S12, ESI†). It is worth noting that although the gold particles supported on SiO_2 are smaller than those supported on GO, the catalytic activity of the former is lower than the latter (Entries 10-13 in Table 1). It indicates that the GO support has a positive influence on the catalytic reaction.[29,30,31] Besides, we synthesized Au/Al_2O_3 composite according to literature[27] and compared its catalytic activity with that of $Au/SiO_2/GO$ composite. The gold particles supported on Al_2O_3 are in the range of 3-7 nm (Fig. S13, ESI†). The TOF values for the styrene epoxidation reaction catalyzed by Au/Al_2O_3 (Entries 14 and 15 in Table 1) are much lower than that catalyzed by the $Au/SiO_2/GO$ catalyst. The possible reason may be that the gold nanoparticles with smaller size have higher activity for the styrene epoxidation.

The $Au/SiO_2/GO$ composites were synthesized at different CO_2 pressures. The gold nanoparticles supported by SiO_2/GO synthesized at 1.14, 3.02, 4.02 and 5.03 MPa are in the range of 2.0-6.0, 2.0-4.0, 2.0-3.0, and 1.4-2.0 nm, respectively (Fig. S14, ESI†). Clearly, the gold nanoparticles are smaller with a narrower size distribution as the pressure is increased. It is noteworthy that in absence of CO_2, the GO sheet is hardly coated by silica and the gold nanoparticles are as large as 50-80 nm (Fig. S15, ESI†). It indicates that CO_2 can promote the deposition of silica on GO nanosheet.

Based on the above results, a mechanism for the formation of $Au/SiO_2/GO$ composite was proposed (Scheme 1). During the synthetic process, TX-100 works as both a reducing agent for Au^{3+} reduction and template (micelle) for forming silica mesopores. CO_2 plays multiple roles as 1) catalyzing TEOS hydrolysis, 2) favoring the formation of small gold nanoparticles due to the viscosity-lowering effect[16], 3) promoting the deposition of both silica on GO nanosheet and gold nanoparticles on SiO_2/GO support due to the enhanced mass transfer.[17] Therefore, by the in situ reaction-deposition process and the subsequent removing of CO_2 and micelles, the mesoporous SiO_2/GO supported gold nanoparticles are formed. Because of the confinement provided by the mesopores of silica layer, the growth or aggregation of gold nanoparticles are restricted largely, resulting in the formation of ultra-small gold nanoparticles. The proposed synthetic route was extended to the formation of $Pd/SiO_2/GO$ composite. The uniform ultra-small Pd nanoparticles (~2 nm) finely dispersed on mesoporous silica/GO nanosheet were formed (Fig. S16, ESI†).

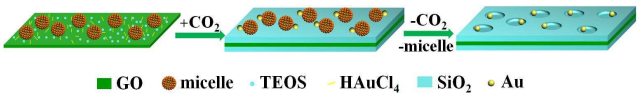

Scheme 1 Schematic illustration for formation of Au/SiO_2/GO composite.

Conclusions

In summary, this work demonstrates the in situ formation of ultra-small gold nanoparticles immobilized on mesoporous SiO_2/GO nanosheet via a one-pot synthetic route. The combination of beneficial features of small gold nanoparticles, mesoporous silica and GO nanosheet of the Au/SiO_2/GO composite makes it excellent candidate of catalyst. We anticipate that this kind of catalyst with unique features would find more promising applications in future.

The authors thank the National Natural Science Foundation of China (21173238, 21133009, U1232203, 21021003), Chinese Academy of Sciences (KJCX2.YW.H16). We are also grateful to Dr. Lirong Zheng, Dr. Jing Zhang and Prof. Yaning Xie of Beijing Synchrotron Radiation Facility (BSRF) for their help on extended X-ray absorption fine structure experiment.

Notes and references

Beijing National Laboratory for Molecular Sciences, CAS Key Laboratory of Colloid and Interface and Thermodynamics, Institute of Chemistry, Chinese Academy of Sciences. Beijing 100190, P.R.China.
Fax: +86-10-62559373; Tel: +86-10-62562821;
E-mail: zhangjl@iccas.ac.cn

† Electronic Supplementary Information (ESI) available: Materials, experimental details, and characterization. See DOI: 10.1039/b000000x/

1 J. A. Farmer and C. T. Campbell, *Science*, 2010, **329**, 933–936.
2 X. Liu, L. He, Y. -M. Liu and Y. Cao, *Acc. Chem. Res.*, 2014, **47**, 793–804.
3 Y. Zhang, X. J. Cui, F. Shi and Y. Q. Deng, *Chem. Rev.*, 2012, **112**, 2467–2505.
4 R. J. White, R. Luque, V. L. Budarin, J. H. Clark and D. J. MacQuarrie, *Chem. Soc. Rev.*, 2009, **38**, 481–486.
5 H. M. Yang, X. J. Cui, Y. Q. Deng and F. Shi. *Chemcatchem*, 2013, **4**, 1739−1743.
6 L. Shang, T. Bian, B. Zhang, D. Zhang, L. -Z. Wu, C. -H. Tung, Y. Yin and T. Zhang, *Angew. Chem. Int. Ed.*, 2014, **53**, 250–254.
7 S. Wang, Q. Zhao, H. Wei, J. -Q. Wang, M. Cho, H. Sung Cho, O. Terasaki and Y. Wan, *J. Am. Chem. Soc.*, 2013, **135**, 11849−11860.
8 J. Pyun, *Angew. Chem. Int. Ed.*, 2008, **50**, 46–48.
9 D. R. Dreyer, S. Park, C. W. Bielawski and R. S. Ruoff, *Chem. Soc. Rev.*, 2010, **39**, 228–240.
10 S. J. Guo, S. J. Dong and E. W. Wang, *ACS Nano*, 2010, **4**, 547–555.
11 X. Zhou, X. Huang, X. Qi, S. Wu, C. Xue, F. Y. C. Boey, Q. Yan, P. Chen and H. Zhang, *J. Phys. Chem. C*, 2009, **113**, 10842–10846.
12 H. M. A. Hassan, V. Abdelsayed, A. S. Khder, K. M. AbouZeid, J. Terner, M. Samy El-Shall, S. I. Al-Resayes and A. A. El-Azhary, *J. Mater. Chem.*, 2009, **19**, 3832–3837.
13 D. Chen, H. B. Feng and J. H. Li, *Chem. Rev.*, 2012, **112**, 6027–6053.
14 D. R. Dreyer, H. -P. Jia and C. W. Bielawski, *Angew. Chemie.*, 2010, **122**, 6965–6968.
15 Y. H. Deng, J. Wei, Z. K. Sun and D. Y. Zhao, *Chem. Soc. Rev.*, 2013, **42**, 4054–4070.
16 P. G. Jessop and B. Subramaniam, *Chem. Rev.*, 2010, **107**, 2666–2694.
17 Y. Zhao, J. Zhang, J. Song, J. Li, J. Liu, T. Wu, P. Zhang and B. Han, *Green Chem.*, 2011, **13**, 2078–2082.
18 J. Hermannsdörfer and R. Kempe, *Chem. Eur. J.*, 2011, **17**, 8071–8077.
19 M. -C. Hsiao, C. -C. M. Ma, J. -C. Chiang, K. -K. Ho, T. -Y. Chou, X. Xie, C. -H. Tsaia, L. -H. Chang and C. -K. Hsieh, *Nanoscale*, 2013, **5**, 5863–5871.
20 V. L. Parola, A. Longo, A. M. Venezia, A. Spinella and E. Caponetti, *Eur. J. Inorg. Chem.*, 2010, 3628–3635.
21 M. L. Pang, J. Y. Hu and H. C. Zeng, *J. Am. Chem. Soc.*, 2010, **132**, 10771–10785.
22 H. -L. Jiang, T. Akita, T. Ishida, M. Haruta and Q. Xu, *J. Am. Chem. Soc.*, 2011, **133**, 1304–1306.
23 Z. Zhang, C. Shao, P. Zou, P. Zhang, M. Zhang, J. Mu, Z. Guo, X. Li, C. Wang and Y. Liu, *Chem. Commun.*, 2011, **47**, 3906–3908.
24 Y. Deng, Y. Cai, Z. Sun, J. Liu, C. Liu, J. Wei, W. Li, C. Liu, Y. Wang and D. Y. Zhao, *J. Am. Chem. Soc.*, 2010, **132**, 8466–8473.
25 D. K. Dumbre, V. R. Choudhary, N. S. Patil, B. S. Uphade and S. K. Bhargava, *J. Colloid Interface Sci.*, 2014, **415**, 111–116.
26 V. R. Choudhary, D. K. Dumbre, N. S. Patil, B. S. Uphade and S. K. Bhargava, *J. Catal.*, 2013, **300**, 217–224.
27 D. Yin, L. Qin, J. Liu, C. Li and Y. Jin, *J. Mol. Catal. A*, 2005, **40**, 40–48.
28 Y. Liu, H. Tsunoyama, T. Akita and T. Tsukuda, *Chem. Commun.*, 2010, **46**, 550–552.
29 G. M. Scheuermann, L. Rumi, P. Steurer, W. Bannwarth and R. Mülhaupt, *J. Am. Chem. Soc.*, 2009, **131**, 8262–8270.
30 L. Shao, X. Huang, D. Teschner and W. Zhang, *ACS Catal.*, 2014, **4**, 2369−2373.
31 C. Su, R. Tandiana, J. Balapanuru, W. Tang, K. Pareek, C. T. Nai, T. Hayashi and K. P. Loh, *J. Am. Chem. Soc.*, 2015, **137**, 685−690.